

# Transcription elongator SPT6L regulates the occupancies of the SWI2/SNF2 chromatin remodelers SYD/BRM and nucleosomes at transcription start sites in Arabidopsis

Jie Shu<sup>1</sup>, Ning Ding<sup>1,5</sup>, Jun Liu<sup>2</sup>, Yuhai Cui<sup>3,4</sup> and Chen Chen<sup>1,5,\*</sup>

<sup>1</sup>Key Laboratory of South China Agricultural Plant Molecular Analysis and Genetic Improvement & Guangdong Provincial Key Laboratory of Applied Botany, South China Botanical Garden, Chinese Academy of Sciences, Guangzhou, Guangdong 510650, China, <sup>2</sup>Agro-biological Gene Research Center, Guangdong Academy of Agricultural Sciences, Guangzhou, Guangdong 510640, China, <sup>3</sup>Agriculture and Agri-Food Canada, London Research and Development Centre, London, Ontario N5V 4T3, Canada, <sup>4</sup>Department of Biology, Western University, London, Ontario N6A 5B7, Canada and <sup>5</sup>University of the Chinese Academy of Sciences, Beijing 100049, China

Received July 06, 2022; Revised October 10, 2022; Editorial Decision October 31, 2022; Accepted November 08, 2022

## ABSTRACT

**Chromatin remodelers have been thought to be crucial in creating an accessible chromatin environment before transcription activation. However, it is still unclear how chromatin remodelers recognize and bind to the active regions. In this study, we found that chromatin remodelers SPLAYED (SYD) and BRAHMA (BRM) interact and co-occupy with Suppressor of Ty6-like (SPT6L), a core subunit of the transcription machinery, at thousands of the transcription start sites (TSS). The association of SYD and BRM to chromatin is dramatically reduced in *spt6l* and can be restored mainly by SPT6LΔtSH2, which binds to TSS in a RNA polymerase II (Pol II)-independent manner. Furthermore, SPT6L and SYD/BRM are involved in regulating the nucleosome and Pol II occupancy around TSS. The presence of SPT6L is sufficient to restore the association of the chromatin remodeler SYD to chromatin and maintain normal nucleosome occupancy. Our findings suggest that the two chromatin remodelers can form protein complexes with the core subunit of the transcription machinery and regulate nucleosome occupancy in the early transcription stage.**

## INTRODUCTION

The cell-type-specific expression of genes is central to numerous biological processes and modulated primarily at the transcription level. In eukaryotic cells, the genomic DNA

wraps around the histone octamer (comprised of two copies of H2A, H2B, H3 and H4) and forms the nucleosome, the fundamental repeating unit of chromatin (1). The tight contacts between nucleosomes and DNA are considered as the major barriers for transcription to proceed (2,3). In eukaryotic cells, multiple mechanisms have been developed to counteract this barrier and ensure efficient Pol II transcription. Generally, three broad classes of such mechanisms have been identified: elongation factors facilitated Pol II activity, chromatin remodelers mediated nucleosome mobilization, and chromatin-modifying factors mediated nucleosome alteration (4–8).

SPT6 is a well-known conserved histone chaperone initially identified by its capacity to maintain genome integrity via the interaction with histones and nucleosome assembly (9,10). In addition, SPT6 serves as an essential transcription elongation factor associated with phosphorylated Pol II during transcription (7,11–13). Mutations in yeast *SPT6* lead to significantly elevated levels of transcripts within coding regions (14,15), implying SPT6's potential role in controlling the precision of transcription initiation. *Arabidopsis thaliana* (Arabidopsis) contains two homologs of SPT6: SPT6 and SPT6L (16). *SPT6* transcript is undetectable in most tissues and mutations in *SPT6* cause invisible defects (16,17), suggesting that it may serve as a pseudogene and thus less studied. *SPT6L*, however, is ubiquitously expressed, and loss of *SPT6L* leads to severe morphological defects (16,18). Similar to other organisms, SPT6L contains a tandem SH2 domain (tSH2), which is required for its association with Pol II (18). In yeast, deletion of the Spt6 Pol II binding domain led to much less recruitment of Spt6 on chromatin (19). However, in plants, the removal of tSH2 domain shifts the binding of

\*To whom correspondence should be addressed. Tel: +86 20 37252711; Email: chenchen101@scbg.ac.cn

SPT6L from gene bodies towards TSS and the introduction of SPT6L $\Delta$ tSH2 into *spt6l* improves the occupancy of Pol II around TSS (18), suggesting its potential role in early transcription.

Chromatin remodelers control access to genomic DNA by noncovalently modifying nucleosome architecture through an ATPase catalytic subunit. Those ATP-dependent chromatin remodelers are evolutionally conserved from yeast to mammals and plants. Based on the ATPase's similarity and difference, those chromatin remodelers are generally divided into four families, namely switching defective/sucrose nonfermenting (SWI/SNF), inositol requiring 80 (INO80), chromodomain helicase DNA binding (CHD), and imitation switch (ISWI) (5,20). Each ATP-dependent chromatin remodeling family performs specialized functions *in vivo*. For example, the SWI/SNF complex alters chromatin accessibility by repositing, ejecting, and sliding nucleosomes (21,22). The INO80 family carries out histone removal and replacement, whereas CHD and ISWI chromatin remodelers mediate nucleosome assembly, spacing, and maturation (23,24).

Originally identified in *Saccharomyces cerevisiae*, the SWI/SNF family contains highly conserved multi-subunit remodelers. Yeast has two SWI/SNF-type ATPases, SWI2/SNF2 and SNF2 homolog 1 (STH1), whereas the *Drosophila* SWI/SNF family contains one ATPase-BRM. Similarly, the human SWI/SNF family has two ATPases, BRM and BRM-related gene 1 (BRG1) (25,26). In Arabidopsis, four SWI2/SNF2-type chromatin remodelers have been discovered, including SYD, BRM, MINUSCULE 1 (MINU1), and MINU2 (20,27). Increasing evidence has shown that Arabidopsis SWI2/SNF2 subunits interact with other chromatin regulators, including histone deacetylase HISTONE DEACETYLASE 2C (HD2C) and histone H3 lysine 27 trimethylation (H3K27me3) demethylase RELATIVE OF EARLY FLOWERING 6 (REF6) (28,29). Our previous work demonstrated that SYD and BRM target to TSS (30), but it remains to be investigated how those chromatin remodelers are recruited to TSS. Early works on yeast shown that numerous chromatin remodelers and histone chaperones coordinate transcription (31–33). Much remains to be clarified on whether and how chromatin remodelers associate with the transcription machinery to promote plant transcription.

In this report, we analyzed the genome-wide association between the transcription elongator SPT6L and the SWI2/SNF2 chromatin remodelers SYD/BRM and found that SPT6L functions as a critical player that bridges chromatin remodelers to the transcription machinery. We provide further evidence showing that SPT6L is required and sufficient for the recruitment of chromatin remodelers at TSS in a Pol II-independent manner and is involved in regulating the nucleosome occupancy around TSS. Taken together, our results suggest a possible scenario that the two chromatin remodelers can directly form protein complexes with the core subunit of transcription machinery and regulate the nucleosome occupancy during early transcription. Our study, therefore, sheds fresh light on mechanisms underlying the transcription initiation in plants.

## MATERIALS AND METHODS

### Plant materials and growth conditions

Transfer DNA (T-DNA) insertion mutants *syd-5* (SALK\_023209) (34), *spt6l* (SALK\_016621) (16,18), *brm-1* (SALK\_030046) (35) and *brm-3* (SALK\_088462) (36) were obtained from the Arabidopsis Biological Resource Center and have been previously reported. All Arabidopsis lines used in this study were in Columbia (Col-0) background. Seeds were stratified in the dark at 4°C for 3 days before being sown on agar plates containing 2.22 g/l Murashige and Skoog basal medium with vitamins mix (Cat. M519, PhytoTech LABS), 1.5% sucrose (pH 5.75), and 0.8% agar (hereafter referred to as 1/2 MS). Plant growth was in long-day photoperiod (16h light/8h dark cycles) at 22°C. All materials used in this study were 10-day old otherwise specified elsewhere. Those transgenic lines *ProSPT6L:SPT6L-GFP*, *ProSPT6L:SPT6L $\Delta$ tSH2-GFP*, *ProSPT6L:SPT6L $\Delta$ tSH2 $\Delta$ YqgF-GFP*, *ProSYD:SYD $\Delta$ C-GFP* and *ProBRM:BRM-GFP* were previously reported (18,30,35). Primers used in this study were listed in Supplementary Dataset S1.

For genotype analyses, *spt6l* seeds were selected from *spt6l*<sup>+/-</sup> based on its defected morphological phenotypes reported previously (16), followed by sown on 1/2 MS plates. To identify *spt6l syd-5* and *spt6l brm-1* double mutants, *spt6l syd-5*<sup>+/-</sup> and *spt6l brm-1*<sup>+/-</sup> seeds were selected from *spt6l*<sup>+/-</sup> *syd-5*<sup>+/-</sup> and *spt6l*<sup>+/-</sup> *brm-1*<sup>+/-</sup>, respectively, and then sown on 1/2 MS plates. On the 10th day, each seedling was taken photos and PCR was then performed to identify *spt6l syd-5* and *spt6l brm-1* seedlings.

### Generation of plasmid constructs

We generated a new binary vector containing a 3× MYC sequence modified from *pMDC123* (hereafter named *m123-MYC*). The previously reported *pMDC107-gSYD* construct was used as the template to amplify a 12 kb genomic sequence, including the *SYD* promoter/regulatory region (30). The PCR product was purified and subcloned into the modified vector *m123-MYC* between the *PmeI* and *PacI* sites. Next, the construct was sequenced to confirm that the *SYD* coding sequence was in-frame. The entry vectors *pDONR221-SPT6L*, *pDONR221-SPT6L $\Delta$ tSH2* and *pDONR221-SPT6L $\Delta$ tSH2 $\Delta$ YqgF*, which were described previously (18), were inserted into the destination vector *pEarleyGate303* according to the manufacturer's instructions (Gateway™ LR Clonase™ II Enzyme mix, Cat. 11791020, Invitrogen). The genomic sequence of *NRPB1* (including 2308 bp upstream of ATG) was amplified and fused a 3× FLAG sequence to its C-terminal, which was then inserted into the *pGreen0029* binary vector. We fused the genomic sequence of *SPT6L* with a glucocorticoid receptor (GR) sequence and a 3× FLAG sequence (*SPT6L-GR*), which was finally inserted into the *pGreen0029* binary vector.

### Plant transformation

The constructs were introduced into *Agrobacterium tumefaciens* strain *GV3101*, which were then transformed into

plants using the floral dip method (37). Homozygous transgenic lines with each homozygous genetic background were selected from the T3 generation, in which the functional tagged proteins were detected.

### Immunoblot and co-immunoprecipitation (Co-IP)

One hundred milligrams of 10-day-old seedlings were harvested and homogenized to fine powder, which was subsequently dissolved in 300  $\mu$ l lysis buffer (100 mM Tris-HCl pH 7.5, 300 mM NaCl, 2 mM EDTA, 1% TritonX-100, 10% glycerol, 1 mM PMSF, and protease inhibitor cocktail) for 30 min at 4°C with gentle shaking. Next, the crude lysate was centrifuged at 18 000 g for 10 min at 4°C to remove debris. For Western blot (WB), the supernatants were mixed with 4 $\times$  SDS loading buffer and loaded onto SDS-PAGE gels. For Co-IP, we added 25  $\mu$ l anti-GFP nanobody agarose beads (Cat. KTSM1301, KT HEALTH) to the supernatants and incubated for 2 h at 4°C with gentle shaking. The interacting proteins were eluted and then loaded onto SDS-PAGE gels. For affinity purification (AP), the lysis buffer excluded EDTA, PMSF, and protease inhibitor cocktail. Then 50  $\mu$ l HisPur Ni-NTA resin (Cat. 88222, Thermo SCIENTIFIC) was added to the supernatants and incubated for 2 h at 4°C with gentle shaking. The His-tagged proteins were eluted and loaded onto SDS-PAGE gels.

The following list is the antibodies used in this study: anti-GFP (Cat. ab290, Abcam; 1:20 000 dilution), anti-H3 (Cat. ab1791, Abcam; 1:20 000 dilution), anti-MYC (Cat. ab9106, Abcam; 1:20 000 dilution), anti-Pol II CTD repeat YSPTSPS (phospho S5) (Cat. ab193467, Abcam; 1:20 000 dilution), anti-RNAPIISer2P (Cat. ab5095, Abcam, 1:20 000 dilution), and anti-DDDDK-tag (Cat. M185, MBL Life science; 1:10 000 dilution).

### Dexamethasone (DEX) treatment

DEX (Cat. D1756, Sigma-Aldrich) was suspended at 20 mM in dimethylsulfoxide (DMSO) and kept at -20°C. In the DEX induction experiments, *spt6l SPT6L-GR SYD-GFP* seeds were sown on 1/2 MS plates containing either 20  $\mu$ M DEX or the equivalent volume of DMSO grown for 10 days. For the short-time DEX induction, *spt6l SPT6L-GR SYD-GFP* seeds were sown on 1/2 MS plates for 10 days, followed by a 1.5 h treatment of 100  $\mu$ M DEX or the equivalent volume of DMSO.

### Cell fractionation

Cell fractionation was performed as described previously (38) with minor modifications. Briefly, approximately 1 gram of seedlings was ground into fine powder and resuspended with 3 ml Honda buffer (0.4 M sucrose, 1.25% Ficoll, 2.5% Dextran T40, 20 mM HEPES (pH 7.5), 10 mM MgCl<sub>2</sub>, 0.5% Triton X-100, 1 mM DTT and protease inhibitor cocktail). After homogenization by gentle rotating at 4°C for 30 min, the solution was filtered through the 40  $\mu$ M cell strainer. We collected 100  $\mu$ l filtrate as the total fraction. The remaining filtrate was centrifuged at 4°C, 2000 g, for 5 min. The supernatant was collected and kept as the cytoplasmic fraction, while the nuclear pellet was

washed with 1 ml Honda buffer three times. Finally, the pellet was retained as the nucleic fraction. For WB, the subcellular fractions were mixed with 4 $\times$  SDS loading buffer and loaded onto SDS-PAGE gels. For Co-IP, the nuclear pellet was dissolved with 300  $\mu$ l lysis buffer (100 mM Tris-HCl pH 7.5, 300 mM NaCl, 2 mM EDTA, 1% TritonX-100, 10% glycerol, 1 mM PMSF, and protease inhibitor cocktail) for 30 min at 4°C with gentle shaking. Then 25  $\mu$ l anti-GFP nanobody agarose beads (Cat. KTSM1301, KT HEALTH) were added to the solution and incubated for 2 h at 4°C with gentle shaking. The interacting proteins were eluted and then loaded onto SDS-PAGE gels.

### Chromatin immunoprecipitation (ChIP)

ChIP assays were carried out as described previously (39–41) with minor modifications. Generally, plants were crosslinked with 1% formaldehyde for 20 min under vacuum at room temperature and quenched with 0.125 M glycine under vacuum for an additional 5 min. Approximately 500 mg of tissues were used for each ChIP assay. The chromatin was sonicated using a Covaris M220 sonicator (peak power: 75; duty factor: 20; cycles/burst: 200) for 210 s at 6°C. The lysates were centrifuged at 18 000 g for 10 min at 4°C to remove debris. Ten microliters of supernatant were used as the input sample, whereas the remaining supernatant was kept for the downstream procedure. Ten microliters of Dynabeads Protein A (Cat. 10002D, ThermoFisher SCIENTIFIC) were added to each sample to prewash for 1 h at 4°C with gentle rotating. ChIP was carried out using antibodies: anti-GFP (Cat. ab290, Abcam) and anti-Pol II CTD repeat YSPTSPS (Cat. ab817, Abcam). Approximately 40  $\mu$ l of Dynabeads Protein A were mixed with 4  $\mu$ l of antibodies and incubated for about 6 h on a rotator at 4°C to form antibody-bead complexes. The prewashed chromatin was incubated with the antibody-bead complexes overnight at 4°C with a slight rotation. The remaining steps were the same as described previously (40). ChIP DNA was used for qPCR with three biological replicates, and results were generated as the percentage of input DNA. The locations of primers on each gene used for qPCR are shown in Supplementary Figure S1. ChIP DNA libraries were prepared following the published protocol (42) with at least two biological replicates otherwise specified elsewhere.

### ChIP-seq data analyses

ChIP-seq data were analyzed as described previously (18,43). Briefly, adapters were removed from raw sequencing reads with cutadapt (version 3.4, -m 10). And the processed reads were mapped to the Arabidopsis genome (TAIR10) by Bowtie2 (44) with default settings. Then PCR duplicates were removed by using samtools (45) (for pair-end reads) or running the MACS2-filterdup program (46,47) (for single-end reads). The reads information of each sample was listed in Supplementary Dataset S2. The correlation between replicates was analyzed and shown in Supplementary Figure S2A, B. To identify read-enriched regions (peaks), the MACS2 program was employed to perform peak calling with the following settings (-g 135000000, -nomodel, and -p 0.01). Highly confident peaks were gener-

ated by running *idr* (2.0.3) (`-idr-threshold 0.01`) with biological replicates. All the peak and gene coordinates were listed in Supplementary Dataset S3. Heatmap and binding profiles were generated using *deeptools* (48). The averaged coverage file from two or three biological replicates was generated by running a GitHub script (<http://wresch.github.io/2014/01/31/mergebigwig-files.html>). Genome tracks were generated with *pyGenomeTracks* (49).

### Micrococcal nuclease (MNase)-qPCR and MNase-seq

The MNase assays were carried out as described previously (50) with minor modifications. Approximately 400 milligrams of seedlings were used per sample. Additionally, equal amounts of spike-in nuclei extracted from *Saccharomyces cerevisiae* were added to each sample before MNase treatment, which worked as the internal control among samples (51). For MNase treatment, the prepared nuclei were resuspended in prewarmed MNase digestion buffer, followed by the addition of 8 units of MNase (Cat. 2910A, TaKaRa) and incubation (15 min at 37°C with periodic agitation). Finally, the mono-nucleosomal DNA was isolated from 2% agarose gels and quantified by the Qubit dsDNA HS assay kit (Cat. Q32851, ThermoFisher SCIENTIFIC).

For MNase-qPCR, the nucleosome occupancy for a specific region was determined as the percentage of input-MNase-digested DNA, which was then normalized to the spike-in-control yeast *NUC6*. Primers used for qPCR are listed in Supplementary Dataset S1. The locations of primers on each gene used for qPCR are shown in Supplementary Figure S1. For MNase-seq, DNA libraries were generated following the published protocol (42).

### MNase-seq data analyses

The raw MNase-seq reads were processed with *cutadapt* (version 3.4, `-m 10`) to remove adaptors. And then, the processed reads were mapped to the Arabidopsis genome (TAIR10) by *Bowtie2* (44) with default settings. The uniquely mapped pairs were obtained by removing unmapped, improperly paired, and duplicated reads using *samtools* (44). The reads information of each sample was listed in Supplementary Dataset S2. The correlation between replicates was analyzed and shown in Supplementary Figure S2C. The nucleosome positions were determined by applying the improved nucleosome-positioning algorithm *iNPS* (52) with default settings. The smoothed bigwig files across biological replicates were generated by using `'dpos'` function in *DANPOS3* (53). Finally, MNase-seq data among samples were normalized by applying quantile normalization methods to normalize occupancy with `'wiq'` function in *DANPOS3*.

## RESULTS

### Genome-wide co-occupancy of SYD and BRM with SPT6L

The TSS occupancy pattern of the SWI2/SNF2 chromatin remodelers SYD and BRM revealed in our recent work (30) resembles the occupancy profile of a truncated version of SPT6L (SPT6LΔtSH2) (18), a core subunit of the transcription machinery. Our previous work indicated that

the introduction of SPT6LΔtSH2 into *spt6l* partially rescues the occupancy of Pol II at TSS, suggesting the potential role of SPT6L in the early transcription stage. As the genome-wide occupancies of SYD, BRM, and SPT6L are associated with the activation of transcription (18,30,54), we were prompted to investigate the relationship among them in the early stage of transcription. By comparing previous ChIP-seq signals (18,28,30), we observed that SYD and BRM co-localized with SPT6LΔtSH2 around TSS at several genes (Figure 1A). We next plotted the ChIP-seq signals of SYD, BRM, SPT6LΔtSH2, and SPT6L at SYD-occupied genes and also found the genome-wide concurrent signals of SYD, BRM and SPT6LΔtSH2 at TSS (Figure 1B). To examine the specificity of co-binding between SWI2/SNF2 and SPT6LΔtSH2, we also plotted four other chromatin remodelers on the same genomic regions and found that except BAF60 (SWI/SNF family) (55), other three chromatin remodelers PHOTOPERIOD INDEPENDENT EARLY FLOWERING 1 (PIE1, SWI2/SNF2-related 1 family) (56), CHROMATIN REMODELING 11 (CHR11, ISWI family) (56), and a putative SNF2-related chromatin remodeler CHR19 (57) were weakly or even not enriched at TSS (Figure 1B). This result suggests that SPT6LΔtSH2 may prefer to interplay with SWI/SNF complex at TSS. To further examine the relationship between SPT6LΔtSH2 and SWI2/SNF2 complex, we found the binding peaks of SYD and BRM largely overlapped with the peaks of SPT6LΔtSH2 (Figure 1C), and the genome-wide ChIP signals of SYD and BRM were positively correlated with that of SPT6LΔtSH2 (Pearson correlation, 0.794 and 0.785, respectively; Supplementary Figure S3). To compare the binding profiles of SYD, BRM, SPT6LΔtSH2, and SPT6L around TSS, we plotted ChIP signals around all SPT6L binding genes and found that except for SPT6L, which were enriched on transcribed regions, the other three proteins were all peaked around TSS (Figure 1D). Interestingly, the peak summits of SYD exactly overlapped with TSS, whereas the peak summits of BRM and SPT6LΔtSH2 were positioned slightly downstream of TSS (Figure 1D). These results suggest that chromatin remodelers SYD and BRM may associate with SPT6L and play roles in early transcription.

### SPT6L bridges chromatin remodelers SYD and BRM to Pol II

Previous work on the purification of transcription elongation complex showed successful purification of multiple chromatin remodelers with transcription elongation factors (17). To further investigate the role of chromatin remodelers in transcription, firstly, we crossed the *SYD-GFP* line with the *spt6l* heterozygous (*spt6l<sup>+/-</sup>*) plant and performed co-IP experiments to examine the interaction of SYD to Pol II in WT and *spt6l* backgrounds (effectiveness of knocking out *SPT6L* was confirmed by qRT-PCR in Supplementary Figure S4A). As shown in Figure 2A and Supplementary Figure S4B, we detected the interaction of SYD with phosphorylated Pol II and found that the interaction was largely compromised in the absence of *SPT6L*, indicating that SPT6L is required for the association of SYD with Pol II. To examine the interaction be-

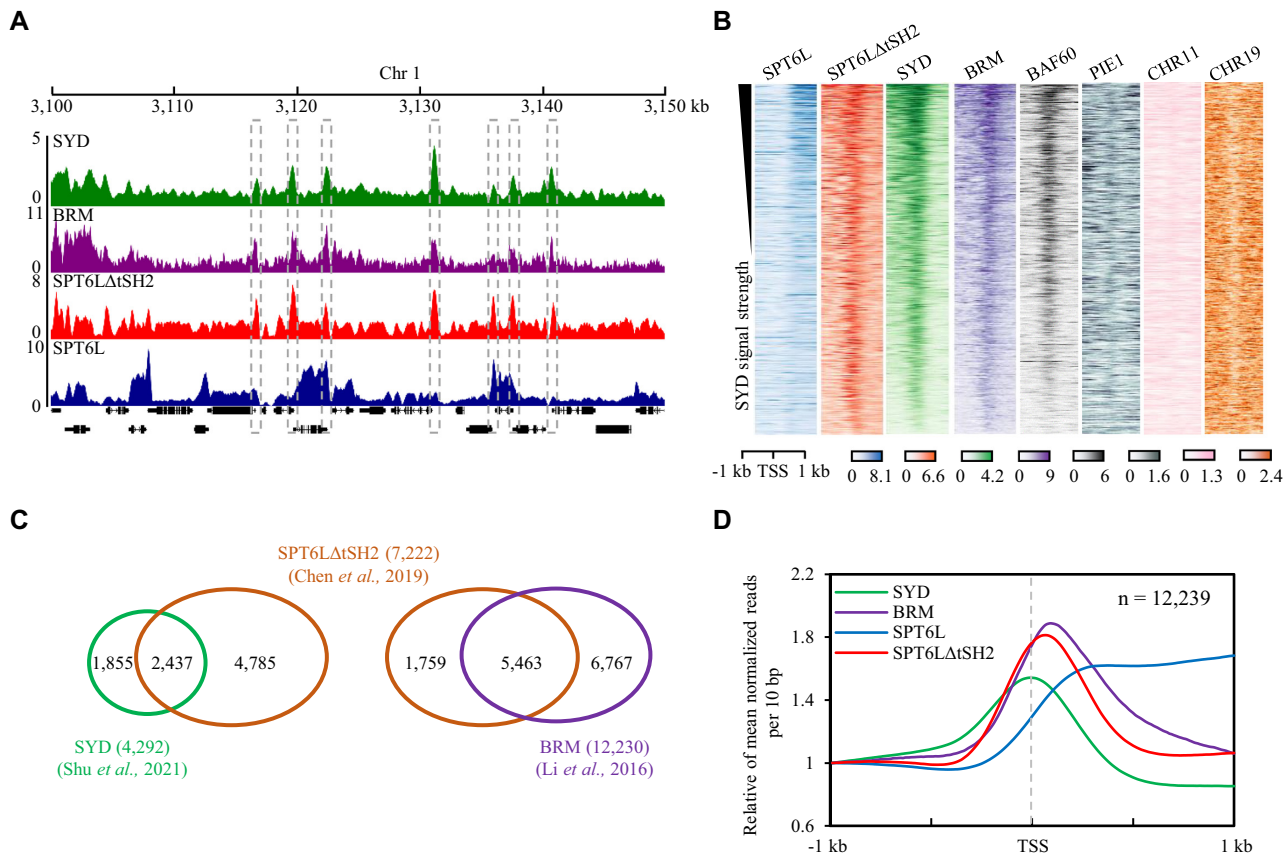


**Figure 1.** SPT6LΔtSH2 co-occupies with the SWI2/SNF2 chromatin remodelers SYD and BRM in Arabidopsis. **(A)** Genome tracks display SYD, BRM, SPT6LΔtSH2, and SPT6L ChIP-seq signals on chromosome 1 (Chr 1: 3100 kb to 3150 kb). The Y-axis values indicate the mean of normalized reads per 10 bp. The dashed rectangles indicate co-binding peaks among examined proteins. **(B)** Heatmaps of SPT6L, SPT6LΔtSH2, SYD, BRM and other reported chromatin remodelers (BAF60, PIE1, CHR11, and CHR19) ChIP signals around transcription start sites (TSS) of all SYD-bound genes. The SYD binding genes were sorted based on the intensity of SYD signals around TSS upstream and downstream 1 kb. **(C)** Venn diagrams indicate the numbers of overlapped peaks between chromatin remodelers (SYD and BRM) and SPT6LΔtSH2. **(D)** Binding profiles of SYD, BRM, SPT6L, and SPT6LΔtSH2 at TSS of all SPT6L binding genes. The plotted regions were around TSS 2 kb (upstream and downstream 1 kb, respectively). The Y-axis value indicates the relative mean of normalized reads per 10 bp. The number of genes was indicated (n).

tween SYD and SPT6L, we crossed the *SYD-GFP* line with the *SPT6LΔtSH2-MYC* and the *SPT6L-MYC* transgenic plants, respectively. We found that SYD interacted with both tSH2 deletion and full-length of SPT6L (Figure 2B), although the latter preferred to associate with gene bodies rather than TSS (Figure 1B, D) (18). The above interactions were further confirmed by co-affinity purification assays (Supplementary Figure S4C). As the tSH2 domain is essential for the association between SPT6L and phosphorylated Pol II (Supplementary Figure S4D) (18) and the present of SPT6LΔtSH2 improves the occupancy of Pol II at TSS (18), the above interactions support a scenario that SPT6L may bridge the association of SYD to phosphorylated Pol II in early transcription. To test this hypothesis, we next investigated the interactions among SYD, SPT6L and Pol II after treating seedlings with the P-TEFb inhibitor, which decreases the phosphorylation levels of Pol II and disrupts its interaction with SPT6L (18,58). As shown in Figure 2C and Supplementary Figure S5A, the application of the inhibitor effectively reduced the phosphorylation level of Pol II within 1 h, but the interactions between SYD and SPT6L were still intact, indicating that phosphorylation of Pol II

may not be required for the formation of the SYD–SPT6L complex.

Since the antibodies of Pol II used were designed to recognize phosphorylated Pol II, it is hard to estimate the interaction between SYD and Pol II after treating with the inhibitor. In addition, the compromised interaction of SYD to phosphorylated Pol II (Figure 2A) may result from the reduction of Pol II phosphorylation in *spt6l*. Therefore, to further examine the interaction between SYD and Pol II, we generated a transgenic line by introducing a transgene of *ProNRPB1:gNRPB1-FLAG* (*NRPB1* encodes the large subunit of Pol II) into *SYD-GFP spt6l<sup>+/-</sup>* plants. By performing the Co-IP experiments, we detected the interaction between SYD and NRPB1 and found that the interaction was dramatically reduced after treatment with the P-TEFb inhibitor, although the amount of NRPB1 was largely unchanged (Figure 2D). Additionally, with the NRPB1-tagged line, we also found that the phosphorylation status of NRPB1 was unaffected in *spt6l* (Supplementary Figure S5B) and confirmed that the interaction between SYD and Pol II was reduced in *spt6l* (Figure 2E and Supplementary Figure S5C). Interestingly, we also found that the introduc-

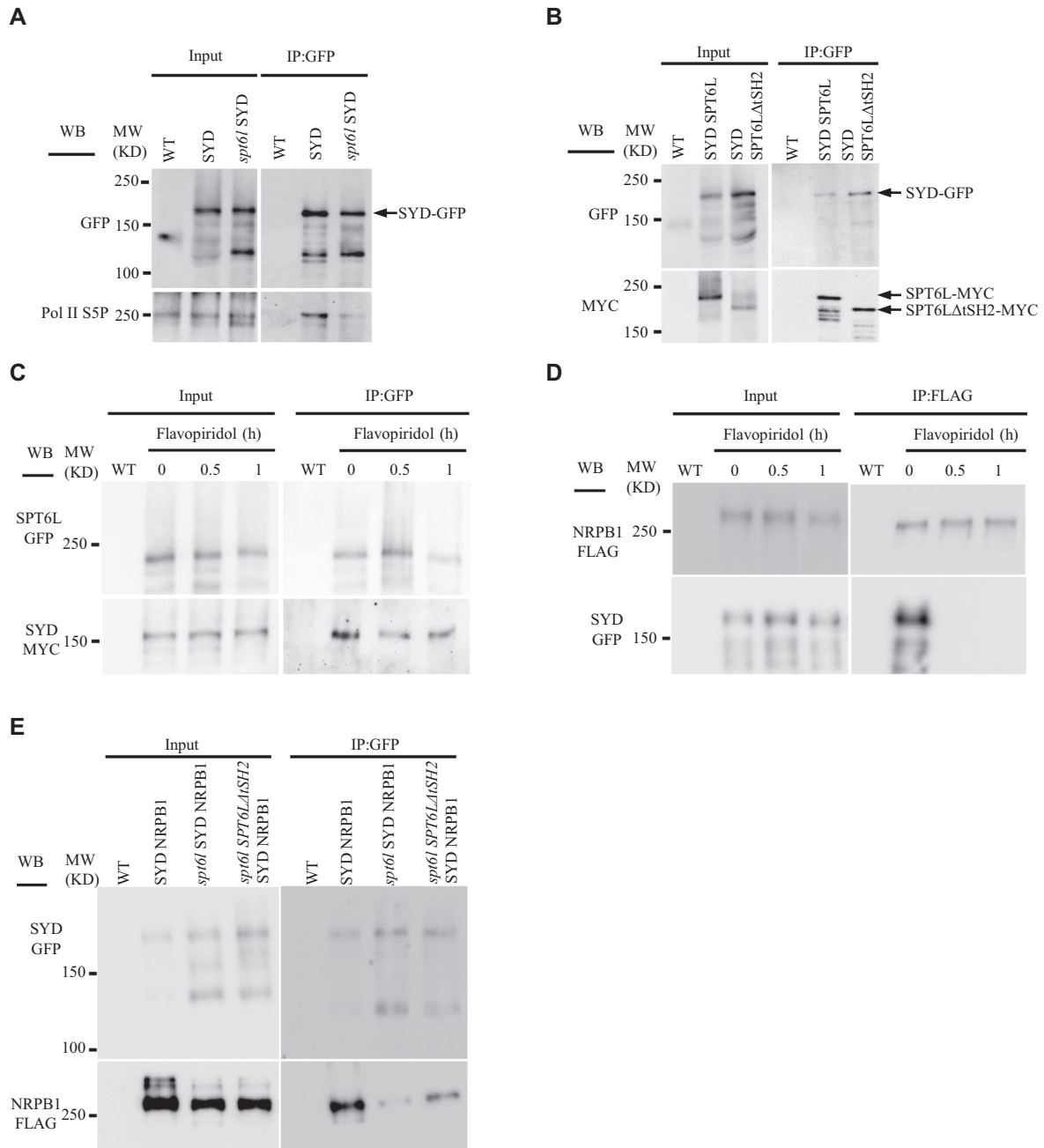


**Figure 2.** SPT6L is required to maintain the interaction between SYD and Pol II. (A) Co-immunoprecipitation (Co-IP) examined the interactions of SYD with serine 5 phosphorylated (CTD) Pol II (Pol II S5P) in WT, *syd-5* SYD-GFP (SYD), and *spt61 syd-5* SYD-GFP (*spt61* SYD). (B) Co-IP performed on *syd-5 spt61* SYD-GFP SPT6L-MYC (SYD SPT6L) and *syd-5* SYD-GFP SPT6LΔtSH2-MYC (SYD SPT6LΔtSH2). (C) Co-IP examined the interactions of SPT6L with SYD after treatment with transcription inhibitor (10 μM flavopiridol) in the indicating period. (D) Co-IP examined the interactions of SYD with NRPB1 after treatment with transcription inhibitor (10 μM flavopiridol) in the indicating period. (E) Co-IP examined the interactions of SYD with NRPB1 in *syd-5* SYD-GFP NRPB1-FLAG (SYD NRPB1), *spt61 syd-5* SYD-GFP NRPB1-FLAG (*spt61* SYD NRPB1), and *spt61 syd-5* SPT6LΔtSH2-MYC SYD-GFP NRPB1-FLAG (*spt61* SPT6LΔtSH2 SYD NRPB1), respectively. IP and Western blot (WB) were performed using specified antibodies.

tion of SPT6LΔtSH2 in *spt61* can partially restore the interaction of SYD to Pol II (Figure 2E), suggesting the existence of other mechanisms to regulate the association between SYD and Pol II. In addition, we detected the interaction of SYD to SPT6LΔtSH2ΔYqgF (Supplementary Figure S5D), which lost its ability to interact with chromatin (18), implying that SYD may form a protein complex with SPT6L independent of chromatin. In summary, these data

indicate that SYD's interaction with SPT6L is independent of Pol II, and SPT6L bridges the association of SYD to Pol II.

As SYD and BRM are closely related chromatin remodelers (24,30,59), we also examined the relationship between BRM and SPT6L. Similar to SYD, BRM interacts with SPT6L in a Pol II-independent manner, and the interaction of BRM with Pol II depends on SPT6L (Supplemen-

tary Figure S6A–E). Moreover, we found that BRM interacts with SPT6L $\Delta$ YqgF (Supplementary Figure S6F), which lost its association with chromatin (18), suggesting that BRM, similar to SYD, may interact with SPT6L independent of chromatin. Altogether, these findings show that SPT6L can form protein complexes with the SWI2/SNF2 chromatin remodelers SYD/BRM and link them to the transcription machinery.

### Genome-wide association of SYD and BRM is mainly dependent on SPT6L

The interaction and co-occupancy of SPT6L with the two chromatin remodelers led us to examine the interplay of their genome-wide recruitment to target genes. We firstly examined the SPT6L genome-wide binding in the *syd-5* null mutant and found that the binding patterns of SPT6L are similar to that in WT (Figure 3A and Supplementary Figure S7A–B), demonstrating that the association of SPT6L with chromatin is not dependent on SYD. On the contrary, the SYD binding signals were dramatically reduced in *spt6l* (Figure 3B–D). As the binding profile of SYD is similar to that of SPT6L $\Delta$ tSH2 (Figure 1A, B) and the interaction between SYD and SPT6L is unaffected after deletion of the tSH2 domain (Figure 2B and Supplementary Figure S4C), we reasoned that the introduction of SPT6L $\Delta$ tSH2 into *spt6l* may rescue the association of SYD to chromatin. Therefore, we profiled the genome-wide binding of SYD in the *spt6l* SPT6L $\Delta$ tSH2 plants and found that the overall occupancy of SYD was partially rescued (Figure 3B–D). These results were further confirmed by ChIP-qPCR analyses at selected genomic loci (Supplementary Figure S7C). To rule out the potential effect of protein stability, we checked the amounts of SYD in WT, *spt6l*, and *spt6l* SPT6L $\Delta$ tSH2 and detected comparable levels of SYD in these genetic backgrounds (Supplementary Figures S5B and S7D). In addition, we examined the dependency of BRM on SPT6L and, as expected, found reduced binding signals of BRM in *spt6l* (Supplementary Figure S7E–H), indicating that SPT6L is required for the recruitment of both SYD and BRM to chromatin.

To clarify the genome-wide dependency of SYD on SPT6L/SPT6L $\Delta$ tSH2, we went through ChIP-seq signals of SYD, SPT6L, and SPT6L $\Delta$ tSH2 and identified 1,556 peaks in SYD (hereafter referred to as SYD alone), which were not overlapped with either SPT6L or SPT6L $\Delta$ tSH2 (Figure 3E). Further, we analyzed the genome features contained in either SYD alone or SYD/SPT6L $\Delta$ tSH2 overlapped peaks and found that the proportion of intergenic region was increased in SYD alone peaks (Supplementary Figure S7I). By comparing ChIP-seq signals of SYD at the above two groups of peaks, we found that stronger ChIP-seq signals at SYD/SPT6L $\Delta$ tSH2 overlapped regions than that at SYD alone regions (Figure 3E). Unexpectedly, the ChIP-seq signals of SYD were decreased and partially recovered both at SYD/SPT6L $\Delta$ tSH2 overlapped and SYD alone peaks (Figure 3E). Similar phenomena were also found in BRM/SPT6L $\Delta$ tSH2 overlapped and BRM alone peaks (Supplementary Figure S7I, J). These results suggest that the genome-wide association of SYD and BRM is likely

contributed by SPT6L and other unknown factors (such as Pol II itself).

To further examine the genetic relationship between SYD/BRM and SPT6L, we identified *spt6l syd-5* and *spt6l brm-1* seedlings from the progenies of double heterozygous plants and compared their morphological phenotypes with each single mutant. As shown in Figure 3F and Supplementary Figure S8, the morphological phenotypes of both *spt6l syd-5* and *spt6l brm-1* in either 10 or 21 days are similar to that of *spt6l*. We then carefully compared and quantified the proportions of abnormal progenies of the three heterozygous (*spt6l*<sup>+/-</sup>, *spt6l*<sup>+/-</sup> *syd-5*<sup>+/-</sup> and *spt6l*<sup>+/-</sup> *brm-1*<sup>+/-</sup>) plants and found that the progenies of *spt6l*<sup>+/-</sup> *syd-5*<sup>+/-</sup> but not *spt6l*<sup>+/-</sup> *brm-1*<sup>+/-</sup> shared similar compositions of abnormal seedlings to that in *spt6l*<sup>+/-</sup> (Figure 3G). These data indicate that the functions of SYD largely depend on SPT6L and BRM may have other independent mechanisms to facilitate its functions.

As we reported previously, the loss of SPT6L dramatically reduced the occupancy of Pol II on chromatin, and SPT6L $\Delta$ tSH2 could partially rescue the Pol II association with TSS (18). Thus, it could be argued that the loss and partially recovered binding signals of SYD in *spt6l* and *spt6l* SPT6L $\Delta$ tSH2, respectively, may be resulted from the changed association of the transcription machinery with chromatin. To examine the potential linkage of SYD with Pol II, we compared the changed occupancies of Pol II and SYD at SYD binding genes after introducing SPT6L $\Delta$ tSH2 into *spt6l* and found that the alterations of Pol II and SYD were not correlated (Figure 3H). In addition, SPT6L mutation resulted in three different changes in Pol II occupancies around SYD-associated TSS: decreased (Group I), unchanged (Group II), and increased (Group III) (Figure 3I). By plotting SYD signals over the three groups of TSS, however, we observed decreased SYD binding signals in all groups (Figure 3I), indicating the occupancy of SYD may not be directly associated with Pol II. Together, our results suggest that SPT6L recruits the SWI2/SNF2 chromatin remodeler SYD at TSS in a Pol II-independent manner.

### SPT6L and SYD/BRM regulate nucleosome occupancy around TSS

As chromatin remodelers play essential roles in the regulation of nucleosome occupancy (59,60), the dependency of SYD and BRM on SPT6L prompted us to further examine the potential roles of SPT6L on the nucleosome arrangement around TSS. By performing MNase digestion followed by high-throughput sequencing (MNase-seq) in WT and *spt6l*, we found that the nucleosome occupancy downstream of TSS was increased in *spt6l* (Figure 4A) and the introduction of SPT6L $\Delta$ tSH2 partially restored the nucleosome occupancy toward the WT level (Figure 4A). To further evaluate the effect of SPT6L on nucleosome arrangement, we characterized different types of nucleosome changes (changes in occupancy, position, and fuzziness) in *spt6l* using the DANPOS3 software (53). As shown in Figure 4B, we detected 50,644 significantly changed (fold change > 2 and  $P < 10^{-5}$ ) nucleosomes within SPT6L-bound regions between WT and *spt6l*. Intriguingly, nearly

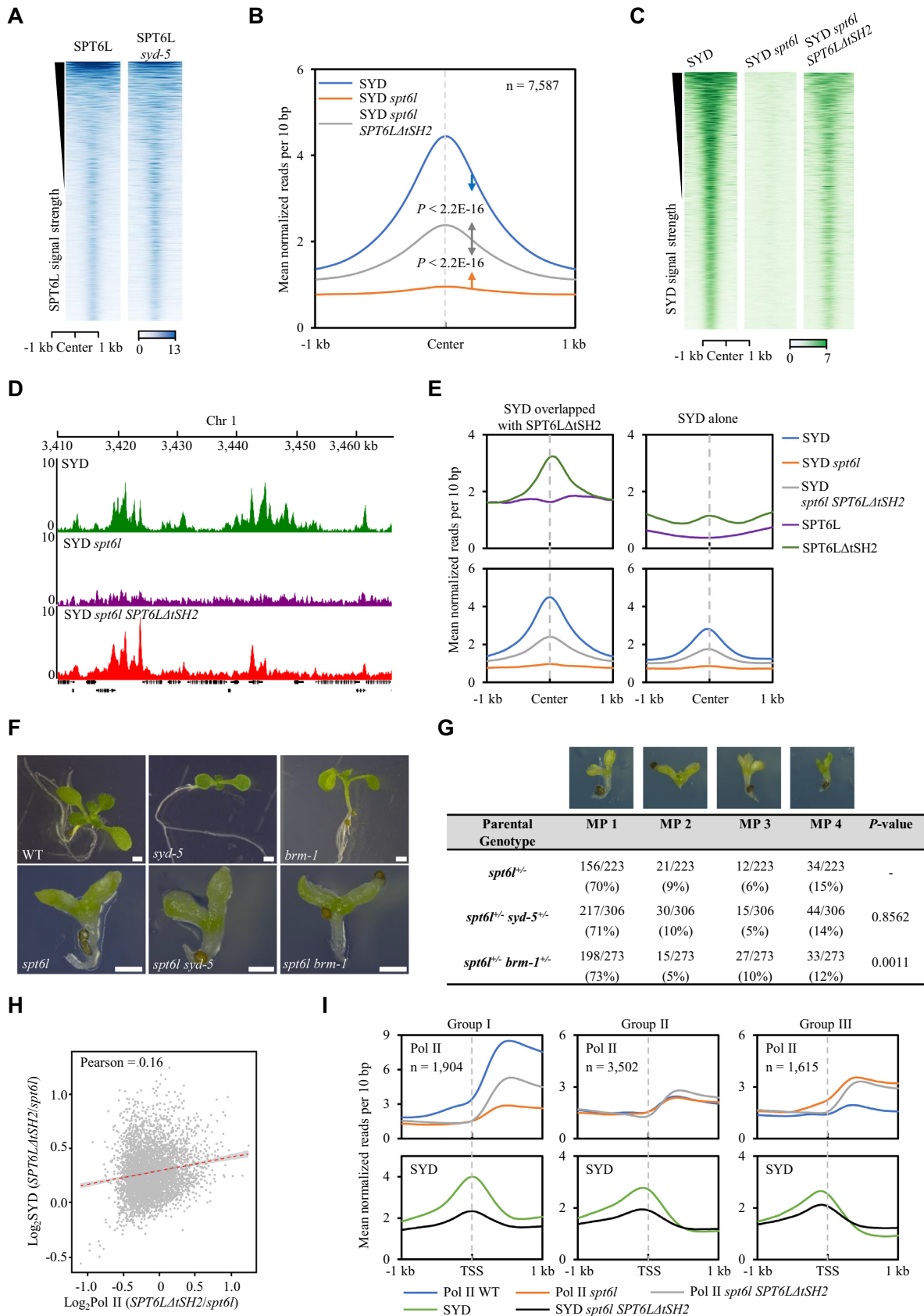


**Figure 3.** Genome-wide association of SYD largely depends on SPT6L. (A) Heatmaps of SPT6L reads measured by CHIP-seq in *spt6l* SPT6L-GFP (SPT6L) and *syd-5 spt6l* SPT6L-GFP (SPT6L *syd-5*) backgrounds over SPT6L binding peaks. From top to bottom, the plotted genomic regions were

half of the changed nucleosomes showed position changes, and the remaining experienced mixed changes (Figure 4B). Indeed, a shifted profile of nucleosome downstream of TSS was observed in *spt6l* by comparing nucleosome occupancy on SPT6L-bound regions (Supplementary Figure S9A). The shifting distances were approximately 30 and 20 bp in upstream and downstream shifts, respectively (Supplementary Figure S9B). To further confirm the nucleosome changes in *spt6l*, we continuously monitored the effect of MNase in WT and *spt6l*. After normalizing with referencing yeast chromatin, we also detected larger amounts of nucleosomes in *spt6l* than that in WT at candidate genes (Figure 4C and Supplementary Figure S9C). To sum up, these results suggest that SPT6L plays a major role in maintaining normal nucleosome occupancy.

Since the lethality of *spt6l* and *syd brm* mutants (18,61), we could not directly assess the nucleosome changes in *spt6l syd*, *spt6l brm*, and *spt6l syd brm*. Instead, we compared the nucleosome changes in *syd-5*, *brm-1*, and *syd-5 brm-3* (*brm-3* severed as a weak allele of *brm-1*) at several SPT6L and SYD/BRM co-binding genes. Consistent with the MNase-seq data, the nucleosome occupancies at the downstream of selected TSS were increased in *spt6l* and rescued in *spt6l SPT6LΔtSH2* (Figure 4D and Supplementary Figure S9D). Furthermore, mutations in the chromatin remodelers SYD/BRM also led to increased nucleosome occupancies at some of the selected genes (Figure 4D and Supplementary Figure S9D), suggesting that both SPT6L and SYD/BRM are involved in the regulation of nucleosome occupancy around TSS.

Nucleosome occupancy at TSS has been linked to transcription activation or repression (62–64). To examine this linkage in *spt6l*, we profiled the MNase-seq reads on previously defined three groups of genes, which showed an increased, unchanged, and decreased Pol II occupancy in *spt6l* (Figure 3I). However, regardless of the Pol II change, we detected increased and partially restored MNase-seq signals in *spt6l* and *spt6l SPT6LΔtSH2*, respectively, in all three groups (Figure 4E). We also analyzed the relationship between Pol II and nucleosome occupancy and did not ob-

serve the correlation of changed Pol II and nucleosome signals in *spt6l* (Figure 4F), suggesting that alteration of nucleosome occupancy may not directly contribute to the association of the transcription machinery. Similarly, we performed Pol II ChIP-seq in *syd-5*, *brm-1* and *syd-5 brm-3* and compared the profiles of Pol II in the three groups of genes as shown in Figure 3I. The occupancies of Pol II at downstream of TSS in *brm-1*, similar to that in *spt6l* (Figure 3I), were slightly decreased and increased in Group I and Group III, respectively (Figure 4G). By comparing the Pol II profiles in *spt6l* and *syd-5 brm-3*, we found that the changed Pol II occupancy in *spt6l* was weakly correlated with that in *syd-5 brm-3* at Group I and Group II genes (Figure 4G), suggesting that SYD/BRM and SPT6L may play similar roles in regulating the occupancy of Pol II around TSS.

### SPT6L is sufficient for recruiting SYD/BRM and restoring nucleosome occupancy

To further examine whether SPT6L is sufficient to bridge SYD/BRM to the transcription machinery and maintain nucleosome occupancy, we fused SPT6L with GR, which can translocate the fused protein into the nucleus upon the application of DEX. We introduced it into *spt6l<sup>+/-</sup>* plants. Under the mock treatment, we observed *spt6l*-like phenotypes in *spt6l ProSPT6L:SPT6L-GR-FLAG* (hereafter referred to as *SPT6L-GR*) seedlings (Figure 5A), and most of the SPT6L-GR protein was indeed trapped in the cytoplasm (Figure 5B). After DEX application, the cytoplasmic SPT6L was translocated into the nucleus (Figure 5B), and the *SPT6L-GR* seedlings were able to develop true leaves (Figure 5A), indicating that the deformed morphology of *spt6l* resulted from the loss-of-nuclear function of SPT6L and the translocated SPT6L was sufficient to rescue the defects of *spt6l* partially. With the inducible system, we next examined the roles of SPT6L in the recruitment of SYD and regulation of nucleosome occupancy. As shown in Figure 5C and Supplementary Figure S10A, under treatment with DEX, the translocated SPT6L could interact with SYD and the association between SYD and Pol II was partially re-

sorted by SPT6L signal strength in *spt6l SPT6L-GFP*. The plotted values are the means of normalized reads ( $1 \times$  sequencing depth normalization) per 10 bp non-overlapped bins, averaged over two biological replicates. (B) Mean density of SYD occupancy in *syd-5 SYD-GFP* (SYD), *spt6l syd-5 SYD-GFP* (SYD *spt6l*), and *spt6l syd-5 SPT6LΔtSH2-MYC SYD-GFP* (SYD *spt6l SPT6LΔtSH2*) at the SYD binding peaks. Y-axis represents the means of normalized reads per 10 bp non-overlapping bins, averaged over three biological replicates. Reads were plotted on 1 kb upstream and downstream of peak summits, respectively. The number of peaks was indicated (n). The significances between SYD against SYD *spt6l* and SYD *spt6l* against SYD *spt6l SPT6LΔtSH2* were calculated by the two-tailed Mann-Whitney test. (C) Heatmaps of SYD reads measured by ChIP-seq in *syd-5 SYD-GFP* (SYD), *spt6l syd-5 SYD-GFP* (SYD *spt6l*), and *spt6l syd-5 SPT6LΔtSH2-MYC SYD-GFP* (SYD *spt6l SPT6LΔtSH2*) backgrounds over the SYD binding peaks. From top to bottom, the plotted genomic regions were sorted by SYD signal strength in *syd-5 SYD-GFP*. The plotted values are the means of normalized reads per 10 bp non-overlapped bins, averaged over three biological replicates. Reads were plotted on 1 kb upstream and downstream of peak summits, respectively. (D) Representative SYD peaks at chromosome 1 (Chr 1: 3410 kb to 3465 kb) to visualize peak changes in *syd-5 SYD-GFP* (SYD), *spt6l syd-5 SYD-GFP* (SYD *spt6l*), and *spt6l syd-5 SPT6LΔtSH2-MYC SYD-GFP* (SYD *spt6l SPT6LΔtSH2*) backgrounds. The ChIP-seq signal of each sample was averaged over three biological replicates. Y-axis represents the means of normalized reads per 10 bp non-overlapping bins. (E) Mean density of SYD occupancy at its binding peaks that overlapped with SPT6LΔtSH2 peaks (1,556 peaks that were randomly selected from the overlapped peaks) and its unique peaks (1556 peaks). Y-axis represents the means of normalized reads per 10 bp non-overlapping bins. Reads were plotted on 1 kb upstream and downstream of peak summits. (F) The morphological phenotypes of 10-day-old WT, *syd-5*, *brm-1*, *spt6l*, *spt6l syd-5*, and *spt6l brm-1* seedlings. Bar = 1 mm. (G) Quantification of the progenies of *spt6l<sup>+/-</sup>*, *spt6l<sup>+/-</sup> syd-5<sup>+/-</sup>*, and *spt6l<sup>+/-</sup> brm-1<sup>+/-</sup>*. The figures indicate four different morphological phenotypes (MP1-4) in abnormal progenies. P values between *spt6l<sup>+/-</sup>* and *spt6l<sup>+/-</sup> syd-5<sup>+/-</sup>* or *spt6l<sup>+/-</sup> brm-1<sup>+/-</sup>* were calculated by Chi-square test. (H) Scatterplot of Pol II and SYD changed ChIP-seq signals at SYD binding genes. Differential SYD (Y-axis) and Pol II (X-axis) ChIP-seq signals ( $\log_2$  fold change) in *spt6l SPT6LΔtSH2* vs. *spt6l* were plotted. (I) Mean density of Pol II and SYD occupancy at the SYD targeted genes, which were grouped into three groups based on the different patterns of Pol II at each gene in WT, *spt6l*, and *spt6l SPT6LΔtSH2*. The number of genes in each group was indicated (n). Y-axis represents the means of normalized reads per 10 bp non-overlapped bins, averaged over two biological replicates. Reads were plotted on 1 kb upstream and downstream of TSS.

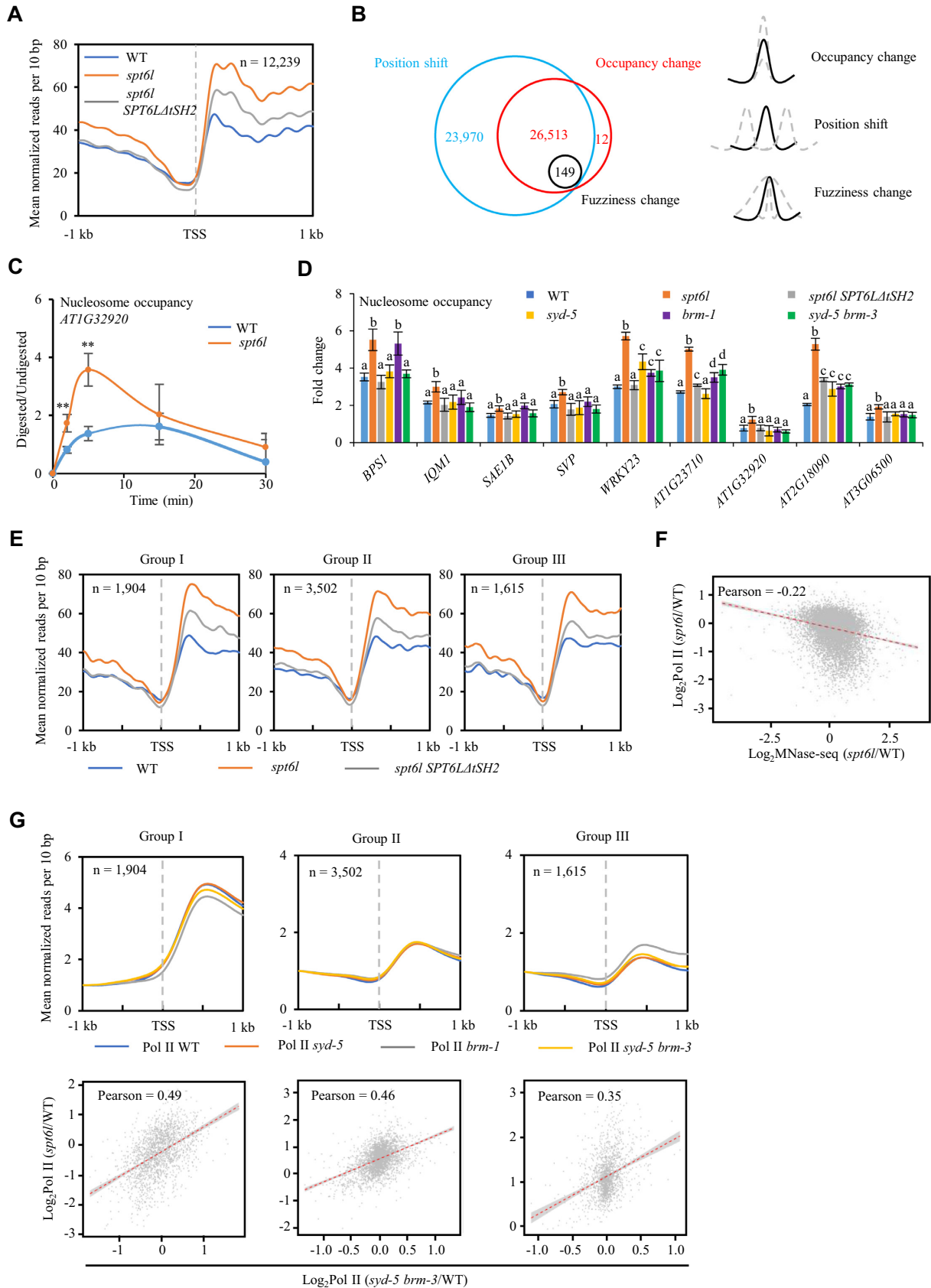


**Figure 4.** SPT6L and SYD/BRM regulate nucleosome occupancy around TSS. (A) Profile plots showing the average MNase-seq signals of WT, *spt6l*, and *spt6l SPT6LΔtSH2* at  $\pm 1$  kb around TSS of SPT6L binding genes. Y-axis represents the means of normalized reads ( $1 \times$  sequencing depth normalization)

stored. The following ChIP and MNase assays showed that the translocated SPT6L could at least partially rescue the occupancy of SYD and nucleosomes at all selected genes (Figure 5D and 5E and Supplementary Figure S10B). In addition, to minimize the indirect effects on SYD recruitment, we also performed the short-time induction (1.5 h) of DEX. As shown in Supplementary Figure S11, the short-time induction was able to translocate SPT6L into nuclei and rescue SYD binding at selected genes (Supplementary Figure S11). However, the nucleosome occupancies at selected genes were not rescued to the level shown in the long-time induction, suggesting that the effectiveness of chromatin remodelers at some loci may take time to be detected. Together, these results indicate that SPT6L is required and sufficient to link the SYD/BRM to chromatin and regulate the nucleosome occupancy during early transcription.

## DISCUSSION

Tightly compacted nucleosomes serve as the primary barrier to transcription initiation and elongation (65). Prior to active transcription, an accessible environment must be created for the assembly of the transcription machinery and its association with chromatin. Therefore, how the arrangement of nucleosomes is precisely regulated during transcription is a key issue for understanding the detailed process of transcription. Our previous work revealed that the conserved transcription elongation factor, SPT6L, can associate with TSS and promote the occupancy of Pol II in Arabidopsis (18). However, how SPT6L facilitates Pol II occupancy around TSS is not clear. In this study, we revealed that SPT6L can interact with the SWI2/SNF2 chromatin remodelers SYD/BRM and bridge them to the transcription machinery. Furthermore, the association between SPT6L and SYD/BRM regulates nucleosome arrangement around TSS and promotes Pol II occupancy. These findings not only provide a new mechanism underlying the recruitment of SWI2/SNF2 chromatin remodelers to the transcription machinery but also reveal how SPT6L mediates Pol II occupancy at the early transcription stage in plants.

It has been known that yeast SPT6 and the FACT complex collaborate to regulate nucleosome occupancy during transcription (66). In combination with our previous work, we found that plant SPT6L associates with TSS (18) and regulates the deposition of the nucleosome (Figure 4A),

suggesting that plant SPT6L, unlike its orthologs in yeast and *Drosophila*, may be involved in the transcription initiation stage. Interestingly, recent work has uncovered that the phosphorylation status of Arabidopsis SPT16, a subunit of the FACT complex, is involved in regulating nucleosome occupancy around TSS (67), suggesting the joint function of SPT6L and FACT on nucleosome regulation during early transcription stage. Additionally, we found an increased nucleosome occupancy around TSS in *spt6l* (Figure 4A), which is inconsistent with reduced nucleosome occupancy after the mutation of *SPT6* in yeast (68). This inconsistency likely results from a comprehensive consequence of compromised SPT6L and chromatin remodelers which associate with the transcription machinery.

Although chromatin remodelers SYD and BRM share similar genome-wide profiles (28,30,54) and show similar functions in controlling plant growth and leaf development (30,69,70), SYD and BRM may present in two distinct complexes. First, SYD and BRM showed different levels of dependency on SPT6L (Figure 3C and Supplementary Figure S7E). The reduced but not eliminated binding signals of BRM in *spt6l* likely result from other recruitment mechanisms, such as the recognition of acetylated histone by its bromodomain (71) and association with other proteins like REF6 (28). Consistent with this notion, the proportions of *spt6l*<sup>+/-</sup>*syd-5*<sup>+/-</sup> but not *spt6l*<sup>+/-</sup>*brm-1*<sup>+/-</sup> progenies are similar to that of *spt6l*<sup>+/-</sup> progenies (Figure 3G) also implies that BRM still partially function in *spt6l*. In addition, the residual BRM binding signals imply that BRM and its associated complex may not directly recruit SYD to chromatin. Second, the genome-wide binding signals of SYD and BRM peaked upstream and downstream of TSS, respectively (Figure 1D). Third, the changed nucleosome occupancies were detected at several genes in *brm-1* rather than *syd-5* (Figure 4D) and the deposition of the nucleosome in *syd-5 brm-3* is similar to that in *brm-1* (Figure 4D), suggesting SYD may present in a different protein complex and be not involved in nucleosome arrangement.

Our previous work reveals the distinct binding profiles of SPT6L and SPT6LΔtSH2, suggesting two different but continuous roles of SPT6L in transcription (18). Both SYD and BRM interact with SPT6L (SYD/BRM-SPT6L), SPT6LΔtSH2 (SYD/BRM-SPT6LΔtSH2), and Pol II (SYD/BRM-Pol II) (Figure 2A-B and Supplementary Figure S6A-C), but the two chromatin remodelers

---

per 10 bp non-overlapping bins, averaged over three biological replicates. The number of genes analyzed was indicated (*n*). (B) Venn diagrams showing the numbers of nucleosomes that exhibit different changes in *spt6l* compared to WT. The changes were subdivided into three types: occupancy change (red), position shift (blue), and fuzziness change (black). (C) MNase-qPCR determined the relative nucleosome occupancy on *AT1G32920* in WT and *spt6l* when digested with MNase in the indicating period. The efficiency of digestion across samples was adjusted according to the level of spik-in yeast *NUC6*. Error bars indicate standard deviations among three biological replicates. Two-tailed Student's *t* test, \*\**P* < 0.01. (D) MNase-qPCR determined the relative nucleosome occupancy on selected genes in different genetic backgrounds. The fold change values across samples were normalized to the level of spik-in yeast *NUC6*. Results were normalized to undigested controls and compared to the value of *NUC6*. Error bars indicate standard deviations among three biological replicates. Lowercase letters indicate significant differences between genetic backgrounds, one-way ANOVA, *P* < 0.05. (E) Profile plots showing the average nucleosome reads signal from WT, *spt6l*, and *spt6l SPT6LΔtSH2* ± 1 kb around TSS in three groups categorized in Figure 3I. Y-axis represents the means of normalized reads per 10 bp non-overlapping bins, averaged over three replicates. The number of peaks analyzed was indicated (*n*). (F) Scatterplot of Pol II and nucleosome changed signals at SPT6L binding genes. Differential Pol II ChIP-seq (Y-axis) and MNase-seq (X-axis) signals (log<sub>2</sub> fold change) in *spt6l* vs. WT were plotted. (G) Top panel: mean density of Pol II occupancy in WT, *syd-5*, *brm-1*, and *syd-5 brm-3*. Y-axis represents the means of normalized reads per 10 bp non-overlapping bins, averaged over two biological replicates (Pol II in *brm-1* with one biological replicate). Reads were plotted on 1 kb upstream and downstream of TSS. The numbers of binding genes were indicated (*n*). The three groups of genes were categorized as shown in Figure 3I. Bottom panel: scatterplot of Pol II changed signals at the three groups of genes showed in the Top panel. Differential Pol II ChIP-seq signals (log<sub>2</sub> fold change) in *spt6l* versus WT (Y-axis) were plotted against that in *syd-5 brm-3* versus WT (X-axis).

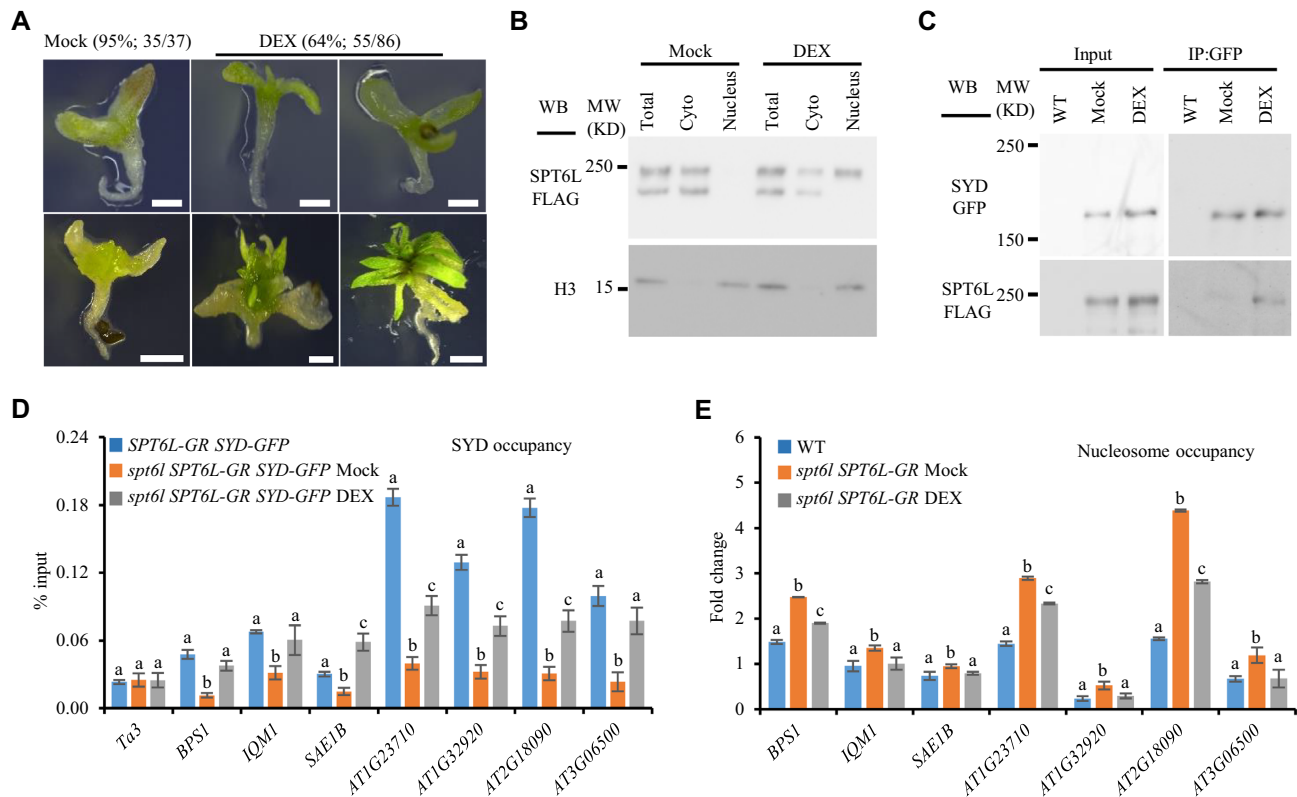


**Figure 5.** SPT6L is sufficient to recruit SYD and restore nucleosome occupancy. (A) The morphological phenotypes of 10-day (top) and 21-day (bottom) old *spt6l SPT6L-GR* seedlings with and without DEX treatment. The percentages indicate the numbers of seedlings with the presented phenotypes divided by the total seedlings. Bar = 1 mm. (B) WB assessing the levels of SPT6L in different cell fractions as indicated with and without DEX treatment. H3 levels served as a loading control and indicator of nucleus proportion. (C) Co-IP examined the interaction of SYD with SPT6L in *spt6l syd-5 SPT6L-GR SYD-GFP* with and without DEX treatment. IP and WB were performed using specified antibodies. (D) ChIP-qPCR examined the SYD occupancy in *syd-5 SPT6L-GR SYD-GFP* (*SPT6L-GR SYD-GFP*) and *spt6l syd-5 SPT6L-GR SYD-GFP* (*spt6l SPT6L-GR SYD-GFP* without/with DEX treatment). ChIP signals are shown as the percentage of input. *Ta3*, a transposable element gene, was used as a negative control locus. Error bars indicate standard deviations among three biological replicates. Lowercase letters indicate significant differences between genetic backgrounds, one-way ANOVA,  $P < 0.05$ . (E) MNase-qPCR determined the fold change of nucleosome occupancy on selected genes in WT and *spt6l SPT6L-GR SYD-GFP* without/with DEX treatment. The fold change values across samples were normalized to the level of spik-in yeast *NUC6*. Error bars indicate standard deviations among three biological replicates. Lowercase letters indicate significant differences between different backgrounds, one-way ANOVA,  $P < 0.05$ .

show enrichment over the TSS regions rather than gene bodies (Figure 1B, D) (28,30,54), suggesting that on one side, SPT6L, as the core subunit of the transcription machinery, may precisely guide chromatin remodelers to active transcription sites and maintain proper nucleosome environment; on the other side, the association between chromatin remodelers and transcription machinery may gradually attenuate during early elongation to productive transcription. Within this transition, the phosphorylation of the Pol II CTD domain (phos-Pol II) plays a critical role and the activities of SPT6 and SPT16 are also regulated in the wave of phosphorylation in yeast and plants, respectively (67,72). By applying the P-TEFb inhibitor, we found that phos-Pol II is required to recruit chromatin remodelers to the transcription machinery (Figure 2D and Supplementary Figure S5A). As the interactions of SYD/BRM-SPT6L were intact after applying the inhibitor (Figure 2C and Supplementary Figure S6D, E), the compromised interactions of SYD/BRM-Pol II may partially result from the reduced interaction between SPT6L and phos-Pol II. Thus, further work is warranted to reveal the dynamic recruitment

of chromatin remodelers to Pol II in different transcription stages.

## DATA AVAILABILITY

The data supporting the findings of this study are available from the corresponding author upon request. The ChIP-seq and MNase-seq data have been deposited in Gene Expression Omnibus with the accession code GSE207391. ChIP-seq and MNase-seq tracks can be directly checked through UCSC browser with the following link (<http://www.genome.ucsc.edu/s/jamwest101/SPT6L%20links%20SYD%20and%20BRM>). The work does not include specialized or in-house scripts and all the parameters for data analyses were provided in the Materials and Methods section.

## SUPPLEMENTARY DATA

Supplementary Data are available at NAR Online.

## ACKNOWLEDGEMENTS

We thank the Arabidopsis Biological Resource Centre for providing the mutant seeds used in this study. The empty vector containing the GR sequence was kindly provided by Dr Xingliang Hou.

Author contributions: C.C. and Y.C. conceived the project; C.C. and J.S. designed the experiments; N.D. performed the western blot experiments; J.S. performed the rest of the experiments; J.S., J.L. and C.C. analyzed ChIP-seq data; C.C. analyzed MNase-seq data, J.S. and C.C. wrote the paper.

## FUNDING

National Natural Science Foundation of China [32070648 to C.C., 32100474 to J.S.]; Natural Science and Engineering Research Council of Canada [RGPIN/04625-561 2017 to Y.C.]; Agriculture and Agri-Food Canada [to Y.C.]. Funding for open access charge: National Natural Science Foundation of China

*Conflict of interest statement.* None declared.

## REFERENCES

- Luger, K., Mader, A.W., Richmond, R.K., Sargent, D.F. and Richmond, T.J. (1997) Crystal structure of the nucleosome core particle at 2.8 Å resolution. *Nature*, **389**, 251–260.
- Bondarenko, V.A., Steele, L.M., Újvári, A., Gaykalova, D.A., Kulaeva, O.I., Polikanov, Y.S., Luse, D.S. and Studitsky, V.M. (2006) Nucleosomes can form a polar barrier to transcript elongation by RNA polymerase II. *Mol. Cell*, **24**, 469–479.
- Lorch, Y., LaPointe, J.W. and Kornberg, R.D. (1987) Nucleosomes inhibit the initiation of transcription but allow chain elongation with the displacement of histones. *Cell*, **49**, 203–210.
- Teves, S.S., Weber, C.M. and Henikoff, S. (2014) Transcribing through the nucleosome. *Trends Biochem. Sci.*, **39**, 577–586.
- Reyes, A.A., Marcum, R.D. and He, Y. (2021) Structure and function of chromatin remodelers. *J. Mol. Biol.*, **433**, 166929.
- Schier, A.C. and Taatjes, D.J. (2020) Structure and mechanism of the RNA polymerase II transcription machinery. *Genes Dev.*, **34**, 465–488.
- Sdano, M.A., Fulcher, J.M., Palani, S., Chandrasekharan, M.B., Parnell, T.J., Whitby, F.G., Formosa, T. and Hill, C.P. (2017) A novel SH2 recognition mechanism recruits Spt6 to the doubly phosphorylated RNA polymerase II linker at sites of transcription. *Elife*, **6**, e28723.
- Kitazawa, T., Machlab, D., Joshi, O., Maiorano, N., Kohler, H., Ducret, S., Kessler, S., Gezelius, H., Sonesson, C., Papisaiikas, P. et al. (2021) A unique bipartite Polycomb signature regulates stimulus-response transcription during development. *Nat. Genet.*, **53**, 379–391.
- Bortvin, A. and Winston, F. (1996) Evidence that Spt6p controls chromatin structure by a direct interaction with histones. *Science*, **272**, 1473–1476.
- Clark-Adams, C.D. and Winston, F. (1987) The SPT6 gene is essential for growth and is required for delta-mediated transcription in *Saccharomyces cerevisiae*. *Mol. Cell Biol.*, **7**, 679–686.
- Sun, M., Lariviere, L., Deng, S., Mayer, A. and Cramer, P. (2010) A tandem SH2 domain in transcription elongation factor Spt6 binds the phosphorylated RNA polymerase II C-terminal repeat domain (CTD). *J. Biol. Chem.*, **285**, 41597–41603.
- Ardehali, M.B., Yao, J., Adelman, K., Fuda, N.J., Petesch, S.J., Webb, W.W. and Lis, J.T. (2009) Spt6 enhances the elongation rate of RNA polymerase II in vivo. *EMBO J.*, **28**, 1067–1077.
- Yoh, S.M., Cho, H., Pickle, L., Evans, R.M. and Jones, K.A. (2007) The Spt6 SH2 domain binds Ser2-P RNAPII to direct Iws1-dependent mRNA splicing and export. *Genes Dev.*, **21**, 160–174.
- Doris, S.M., Chuang, J., Viktorovskaya, O., Murawska, M., Spatt, D., Churchman, L.S. and Winston, F. (2018) Spt6 is required for the fidelity of promoter selection. *Mol. Cell*, **72**, 687–699.
- Kaplan, C.D., Laprade, L. and Winston, F. (2003) Transcription elongation factors repress transcription initiation from cryptic sites. *Science*, **301**, 1096–1099.
- Gu, X.L., Wang, H., Huang, H. and Cui, X.F. (2012) SPT6L encoding a putative WG/GW-repeat protein regulates apical-basal polarity of embryo in Arabidopsis. *Mol. Plant*, **5**, 249–259.
- Antosz, W., Pfab, A., Ehrnsberger, H.F., Holzinger, P., Köllen, K., Mortensen, S.A., Bruckmann, A., Schubert, T., Längst, G., Griesenbeck, J. et al. (2017) The composition of the Arabidopsis RNA polymerase II transcript elongation complex reveals the interplay between elongation and mRNA processing factors. *Plant Cell*, **29**, 854–870.
- Chen, C., Shu, J., Li, C., Thapa, R.K., Nguyen, V., Yu, K., Yuan, Z.C., Kohalmi, S.E., Liu, J., Marsolais, F. et al. (2019) RNA polymerase II-independent recruitment of SPT6L at transcription start sites in Arabidopsis. *Nucleic Acids Res.*, **47**, 6714–6725.
- Mayer, A., Lidschreiber, M., Siebert, M., Leike, K., Soding, J. and Cramer, P. (2010) Uniform transitions of the general RNA polymerase II transcription complex. *Nat. Struct. Mol. Biol.*, **17**, 1272–1278.
- Ojolo, S.P., Cao, S., Priyadarshani, S.V.G.N., Li, W., Yan, M., Aslam, M., Zhao, H. and Qin, Y. (2018) Regulation of plant growth and development: a review from a chromatin remodeling perspective. *Front. Plant Sci.*, **9**, 1232.
- Li, M., Hada, A., Sen, P., Olufemi, L., Hall, M.A., Smith, B.Y., Forth, S., McKnight, J.N., Patel, A., Bowman, G.D. et al. (2015) Dynamic regulation of transcription factors by nucleosome remodeling. *Elife*, **4**, e06249.
- Schwabish, M.A. and Struhl, K. (2007) The Swi/Snf complex is important for histone eviction during transcriptional activation and RNA polymerase II elongation in vivo. *Mol. Cell Biol.*, **27**, 6987–6995.
- Kobayashi, W. and Kurumizaka, H. (2019) Structural transition of the nucleosome during chromatin remodeling and transcription. *Curr. Opin. Struct. Biol.*, **59**, 107–114.
- Han, S.K., Wu, M.F., Cui, S. and Wagner, D. (2015) Roles and activities of chromatin remodeling ATPases in plants. *Plant J.*, **83**, 62–77.
- St. Pierre, R. and Kadoch, C. (2017) Mammalian SWI/SNF complexes in cancer: emerging therapeutic opportunities. *Curr. Opin. Genet. Dev.*, **42**, 56–67.
- Clapier, C.R. and Cairns, B.R. (2009) The biology of chromatin remodeling complexes. *Annu. Rev. Biochem.*, **78**, 273–304.
- Sang, Y., Silva-Ortega, C.O., Wu, S., Yamaguchi, N., Wu, M.-F., Pfluger, J., Gillmor, C.S., Gallagher, K.L. and Wagner, D. (2012) Mutations in two non-canonical Arabidopsis SWI2/SNF2 chromatin remodeling ATPases cause embryogenesis and stem cell maintenance defects. *Plant J.*, **72**, 1000–1014.
- Li, C., Gu, L., Gao, L., Chen, C., Wei, C.Q., Qiu, Q., Chien, C.W., Wang, S., Jiang, L., Ai, L.F. et al. (2016) Concerted genomic targeting of H3K27 demethylase REF6 and chromatin-remodeling ATPase BRM in Arabidopsis. *Nat. Genet.*, **48**, 687–693.
- Buszewicz, D., Archacki, R., Palusiński, A., Kotliński, M., Fogtman, A., Iwanicka-Nowicka, R., Sosnowska, K., Kuciński, J., Pupel, P., Ołędzki, J. et al. (2016) HD2C histone deacetylase and a SWI/SNF chromatin remodelling complex interact and both are involved in mediating the heat stress response in Arabidopsis. *Plant Cell Environ.*, **39**, 2108–2122.
- Shu, J., Chen, C., Li, C., Thapa, R.K., Song, J., Xie, X., Nguyen, V., Bian, S., Liu, J., Kohalmi, S.E. et al. (2021) Genome-wide occupancy of Arabidopsis SWI/SNF chromatin remodeler SPLAYED provides insights into its interplay with its close homolog BRAHMA and Polycomb proteins. *Plant J.*, **106**, 200–213.
- Erkina, T.Y. and Erkin, A. (2015) ASF1 and the SWI/SNF complex interact functionally during nucleosome displacement, while FACT is required for nucleosome reassembly at yeast heat shock gene promoters during sustained stress. *Cell Stress Chaperones*, **20**, 355–369.
- Zhang, L., Fletcher, A.G.L., Cheung, V., Winston, F. and Stargell, L.A. (2008) Spn1 regulates the recruitment of Spt6 and the Swi/Snf complex during transcriptional activation by RNA Polymerase II. *Mol. Cell Biol.*, **28**, 1393–1403.
- Walfridsson, J., Khorosjutina, O., Matikainen, P., Gustafsson, C.M. and Ekwall, K. (2007) A genome-wide role for CHD remodelling factors and Nap1 in nucleosome disassembly. *EMBO J.*, **26**, 2868–2879.

34. Walley, J.W., Rowe, H.C., Xiao, Y., Chehab, E.W., Kliebenstein, D.J., Wagner, D. and Dehesh, K. (2008) The chromatin remodeler SPLAYED regulates specific stress signaling pathways. *PLoS Pathog.*, **4**, e1000237.
35. Li, C., Chen, C., Gao, L., Yang, S., Nguyen, V., Shi, X., Siminovich, K., Kohalmi, S.E., Huang, S., Wu, K. *et al.* (2015) The Arabidopsis SWI2/SNF2 chromatin remodeler BRAHMA regulates Polycomb function during vegetative development and directly activates the flowering repressor gene *SVP*. *PLoS Genet.*, **11**, e1004944.
36. Tang, X., Hou, A., Babu, M., Nguyen, V., Hurtado, L., Lu, Q., Reyes, J.C., Wang, A., Keller, W.A., Harada, J.J. *et al.* (2008) The Arabidopsis BRAHMA chromatin-remodeling ATPase is involved in repression of seed maturation genes in leaves. *Plant Physiol.*, **147**, 1143–1157.
37. Zhang, X., Henriques, R., Lin, S.S., Niu, Q.-W. and Chua, N.-H. (2006) Agrobacterium-mediated transformation of Arabidopsis thaliana using the floral dip method. *Nat. Protoc.*, **1**, 641–646.
38. Long, Y., Jia, J., Mo, W., Jin, X. and Zhai, J. (2021) FLEP-seq: simultaneous detection of RNA polymerase II position, splicing status, polyadenylation site and poly(A) tail length at genome-wide scale by single-molecule nascent RNA sequencing. *Nat. Protoc.*, **16**, 4355–4381.
39. Zhao, L., Xie, L., Zhang, Q., Ouyang, W., Deng, L., Guan, P., Ma, M., Li, Y., Zhang, Y., Xiao, Q. *et al.* (2020) Integrative analysis of reference epigenomes in 20 rice varieties. *Nat. Commun.*, **11**, 2658.
40. Gendrel, A.-V., Lippman, Z., Martienssen, R. and Colot, V. (2005) Profiling histone modification patterns in plants using genomic tiling microarrays. *Nat. Methods*, **2**, 213–218.
41. Shu, J., Chen, C., Thapa, R.K., Bian, S., Nguyen, V., Yu, K., Yuan, Z.-C., Liu, J., Kohalmi, S.E., Li, C. *et al.* (2019) Genome-wide occupancy of histone H3K27 methyltransferases CURLY LEAF and SWINGER in Arabidopsis seedlings. *Plant Direct*, **3**, e00100.
42. Meers, M.P., Bryson, T.D., Henikoff, J.G. and Henikoff, S. (2019) Improved CUT&RUN chromatin profiling tools. *Elife*, **8**, e46314.
43. Chen, C., Li, C., Wang, Y., Renaud, J., Tian, G., Kambhampati, S., Saatian, B., Nguyen, V., Hannoufa, A., Marsolais, F. *et al.* (2017) Cytosolic acetyl-CoA promotes histone acetylation predominantly at H3K27 in Arabidopsis. *Nat. Plants*, **3**, 814–824.
44. Langmead, B. and Salzberg, S.L. (2012) Fast gapped-read alignment with Bowtie 2. *Nat. Methods*, **9**, 357–359.
45. Danecek, P., Bonfield, J.K., Liddle, J., Marshall, J., Ohan, V., Pollard, M.O., Whitwham, A., Keane, T., McCarthy, S.A., Davies, R.M. *et al.* (2021) Twelve years of SAMtools and BCFtools. *Gigascience*, **10**, giab008.
46. Zhang, Y., Liu, T., Meyer, C.A., Eeckhoutte, J., Johnson, D.S., Bernstein, B.E., Nussbaum, C., Myers, R.M., Brown, M., Li, W. *et al.* (2008) Model-based analysis of ChIP-seq (MACS). *Genome Biol.*, **9**, R137.
47. Feng, J., Liu, T., Qin, B., Zhang, Y. and Liu, X.S. (2012) Identifying ChIP-seq enrichment using MACS. *Nat. Protoc.*, **7**, 1728–1740.
48. Ramirez, F., Ryan, D.P., Gruning, B., Bhardwaj, V., Kilpert, F., Richter, A.S., Heyne, S., Dundar, F. and Manke, T. (2016) deepTools2: a next generation web server for deep-sequencing data analysis. *Nucleic Acids Res.*, **44**, W160–W165.
49. Lopez-Delisle, L., Rabbani, L., Wolff, J., Bhardwaj, V., Backofen, R., Gruning, B., Ramirez, F. and Manke, T. (2021) pyGenomeTracks: reproducible plots for multivariate genomic datasets. *Bioinformatics*, **37**, 422–423.
50. Li, G., Liu, S., Wang, J., He, J., Huang, H., Zhang, Y. and Xu, L. (2014) ISWI proteins participate in the genome-wide nucleosome distribution in Arabidopsis. *Plant J.*, **78**, 706–714.
51. Chereji, R.V., Bryson, T.D. and Henikoff, S. (2019) Quantitative MNase-seq accurately maps nucleosome occupancy levels. *Genome Biol.*, **20**, 198.
52. Chen, W., Liu, Y., Zhu, S., Green, C.D., Wei, G. and Han, J.D. (2014) Improved nucleosome-positioning algorithm iNPS for accurate nucleosome positioning from sequencing data. *Nat. Commun.*, **5**, 4909.
53. Chen, K., Xi, Y., Pan, X., Li, Z., Kaestner, K., Tyler, J., Dent, S., He, X. and Li, W. (2013) DANPOS: dynamic analysis of nucleosome position and occupancy by sequencing. *Genome Res.*, **23**, 341–351.
54. Archacki, R., Yatusevich, R., Buszewicz, D., Krzyczmonik, K., Patryn, J., Iwanicka-Nowicka, R., Biecek, P., Wilczynski, B., Koblowska, M., Jerzmanowski, A. *et al.* (2017) Arabidopsis SWI/SNF chromatin remodeling complex binds both promoters and terminators to regulate gene expression. *Nucleic Acids Res.*, **45**, 3116–3129.
55. Jégu, T., Veluchamy, A., Ramirez-Prado, J.S., Rizzi-Paillet, C., Perez, M., Lhomme, A., Latrasse, D., Coleno, E., Vicaire, S., Legras, S. *et al.* (2017) The Arabidopsis SWI/SNF protein BAF60 mediates seedling growth control by modulating DNA accessibility. *Genome Biol.*, **18**, 114.
56. Luo, Y.X., Hou, X.M., Zhang, C.J., Tan, L.M., Shao, C.R., Lin, R.N., Su, Y.N., Cai, X.W., Li, L., Chen, S. *et al.* (2020) A plant-specific SWR1 chromatin-remodeling complex couples histone H2A.Z deposition with nucleosome sliding. *EMBO J.*, **39**, e102008.
57. Kang, H., Liu, Y., Fan, T., Ma, J., Wu, D., Heitz, T., Shen, W.H. and Zhu, Y. (2022) Arabidopsis CHROMATIN REMODELING 19 acts as a transcriptional repressor and contributes to plant pathogen resistance. *Plant Cell*, **34**, 1100–1116.
58. Zhu, J., Liu, M., Liu, X. and Dong, Z. (2018) RNA polymerase II activity revealed by GRO-seq and pNET-seq in Arabidopsis. *Nat. Plants*, **4**, 1112–1123.
59. Yang, T., Wang, D., Tian, G., Sun, L., Yang, M., Yin, X., Xiao, J., Sheng, Y., Zhu, D., He, H. *et al.* (2022) Chromatin remodeling complexes regulate genome architecture in Arabidopsis. *Plant Cell*, **34**, 2638–2651.
60. Torres, E.S. and Deal, R.B. (2019) The histone variant H2A.Z and chromatin remodeler BRAHMA act coordinately and antagonistically to regulate transcription and nucleosome dynamics in Arabidopsis. *Plant J.*, **99**, 144–162.
61. Bezhani, S., Winter, C., Hershman, S., Wagner, J.D., Kennedy, J.F., Kwon, C.S., Pfluger, J., Su, Y. and Wagner, D. (2007) Unique, shared, and redundant roles for the Arabidopsis SWI/SNF chromatin remodeling ATPases BRAHMA and SPLAYED. *Plant Cell*, **19**, 403–416.
62. Asthana, A., Ramanan, P., Hirschi, A., Guiley, K.Z., Wijeratne, T.U., Shelansky, R., Doody, M.J., Narasimhan, H., Boeger, H., Tripathi, S. *et al.* (2022) The MuvB complex binds and stabilizes nucleosomes downstream of the transcription start site of cell-cycle dependent genes. *Nat. Commun.*, **13**, 526.
63. Jiang, Z. and Zhang, B. (2021) On the role of transcription in positioning nucleosomes. *PLoS Comput. Biol.*, **17**, e1008556.
64. Kubik, S., O'Duibhir, E., de Jonge, W.J., Mattarocci, S., Albert, B., Falcone, J.-L., Bruzzone, M.J., Holstege, F.C.P. and Shore, D. (2018) Sequence-directed action of RSC remodeler and general regulatory factors modulates +1 nucleosome position to facilitate transcription. *Mol. Cell*, **71**, 89–102.
65. Kujirai, T. and Kurumizaka, H. (2020) Transcription through the nucleosome. *Curr. Opin. Struct. Biol.*, **61**, 42–49.
66. Duina, A.A. (2011) Histone chaperones Spt6 and FACT: similarities and differences in modes of action at transcribed genes. *Genet. Res. Int.*, **2011**, 625210.
67. Michl-Holzinger, P., Obermeyer, S., Markusch, H., Pfab, A., Ettner, A., Bruckmann, A., Babl, S., Langst, G., Schwartz, U., Tvardovskiy, A. *et al.* (2022) Phosphorylation of the FACT histone chaperone subunit SPT16 affects chromatin at RNA polymerase II transcriptional start sites in Arabidopsis. *Nucleic Acids Res.*, **50**, 5014–5028.
68. DeGennaro, C.M., Alver, B.H., Marguerat, S., Stepanova, E., Davis, C.P., Bahler, J., Park, P.J. and Winston, F. (2013) Spt6 regulates intragenic and antisense transcription, nucleosome positioning, and histone modifications genome-wide in fission yeast. *Mol. Cell Biol.*, **33**, 4779–4792.
69. Wu, M.F., Yamaguchi, N., Xiao, J., Bargmann, B., Estelle, M., Sang, Y. and Wagner, D. (2015) Auxin-regulated chromatin switch directs acquisition of flower primordium founder fate. *Elife*, **4**, e09269.
70. Kwon, C.S., Hibara, K.i., Pfluger, J., Bezhani, S., Metha, H., Aida, M., Tasaka, M. and Wagner, D. (2006) A role for chromatin remodeling in regulation of CUC gene expression in the Arabidopsis cotyledon boundary. *Development*, **133**, 3223–3230.
71. Yu, Y., Fu, W., Xu, J., Lei, Y., Song, X., Liang, Z., Zhu, T., Liang, Y., Hao, Y., Yuan, L. *et al.* (2021) Bromodomain-containing proteins BRD1, BRD2, and BRD13 are core subunits of SWI/SNF complexes and vital for their genomic targeting in Arabidopsis. *Mol. Plant*, **14**, 888–904.
72. Gouot, E., Bhat, W., Rufiange, A., Fournier, E., Paquet, E. and Nourani, A. (2018) Casein kinase 2 mediated phosphorylation of Spt6 modulates histone dynamics and regulates spurious transcription. *Nucleic Acids Res.*, **46**, 7612–7630.